Journal of Materials Chemistry B

Distinguishing anti-PEG antibodies by specificity for the PEG terminus using nanoarchitectonics-based antibiofouling cello-oligosaccharide platforms

Journal:	*Journal of Materials Chemistry B*
Manuscript ID	TB-ART-07-2023-001723.R1
Article Type:	Paper
Date Submitted by the Author:	17-Nov-2023
Complete List of Authors:	Sugiura, Kai; Tokyo Institute of Technology, Department of Chemical Science and Engineering Sawada, Toshiki; Tokyo Institute of Technology, Department of Chemical Science and Engineering Hata, Yuuki; Tokyo Institute of Technology, Department of Chemical Science and Engineering Tanaka, Hiroshi; Tokyo Institute of Technology, Chemical Science and Engineering Serizawa, Takeshi; Tokyo Institute of Technology, Department of Chemical Science and Engineering

Distinguishing anti-PEG antibodies by specificity for the PEG terminus using nanoarchitectonics-based antibiofouling cello-oligosaccharide platforms†

Kai Sugiura, Toshiki Sawada, Yuuki Hata, Hiroshi Tanaka and Takeshi Serizawa*

Department of Chemical Science and Engineering, School of Materials and Chemical Technology, Tokyo Institute of Technology, 2-12-1 Ookayama, Meguro-ku, Tokyo 152-8550, Japan. E-mail address: serizawa@mac.titech.ac.jp

† Electronic supplementary information (ESI) available.

ABSTRACT

The conjugation of poly(ethylene glycol) (PEG) to therapeutic proteins or nanoparticles is a widely used pharmaceutical strategy to improve their therapeutic efficacy. However, conjugation can make PEG immunogenic and induce the production of anti-PEG antibodies, which decreases both the therapeutic efficacy after repeated dosing and clinical safety. To address these concerns, it is

essential to analyze the binding characteristics of anti-PEG antibodies to PEG. However, distinguishing anti-PEG antibodies is still a difficult task. Herein, we demonstrate the use of antibiofouling cello-oligosaccharide assemblies tethering one-terminal methoxy oligo(ethylene glycol) (OEG) ligands for distinguishing anti-PEG antibodies in a simple manner. The OEG ligand-tethering two-dimensional crystalline cello-oligosaccharide assemblies were stably dispersed in a buffer solution and had antibiofouling properties against nonspecific protein adsorption. These characteristics allowed enzyme-linked immunosorbent assays (ELISAs) to be simply performed by cycles of centrifugation/redispersion of aqueous dispersions of the assemblies. The simple assays revealed that the specific OEG ligand-tethering assemblies could distinguish anti-PEG antibodies to detect a specific antibody that preferentially binds to the methoxy terminus of the PEG chain with 3 repeating ethylene glycol units. Furthermore, quantitative detection of the antibodies was successfully performed with high sensitivity even in the presence of serum. The detectable and quantifiable range of antibody concentrations covered those required clinically. Our findings open a new avenue for analyzing the binding characteristics of anti-PEG antibodies in biological samples.

1. Introduction

The conjugation of poly(ethylene glycol) (PEG) to therapeutic proteins or nanoparticles, such as liposomes and lipid nanoparticles, which is termed PEGylation, prolongs the blood circulation time of the therapeutic component and shields immunogenic epitopes on the protein.[1–3] More than twenty PEGylated drugs and nanoparticles have been approved by the US Food and Drug Administration (FDA) for clinical applications. Generally, PEG is a biocompatible water-soluble polymer; however, once conjugated to drugs and nanoparticles, PEG has actually been

demonstrated to be weakly immunogenic and can induce the production of anti-PEG antibodies.[4,5] Anti-PEG antibodies are also found in healthy people who have never been exposed to PEGylated therapeutics but to forms of PEG in daily products, such as cosmetics, shampoos, and toothpastes.[6,7] The retention of anti-PEG antibodies in patients potentially hinders the therapeutic efficacy and safety of PEGylated therapeutics. Anti-PEG antibodies interact with PEGylated therapeutics to form complexes that activate complement and cause an accelerated blood clearance (ABC) phenomenon.[8,9] Moreover, anti-PEG antibodies may cause severe allergic reactions in some individuals upon the administration of PEGylated therapeutics, including PEGylated protein drugs and COVID-19 mRNA vaccines.[10–12]

To develop technologies that reduce the adverse effects of PEGylated therapeutics, it is essential to analyze the binding characteristics of anti-PEG antibodies to PEG. Anti-PEG antibodies are a group of antibodies that recognize different parts of PEG chains and are broadly classified into two groups: backbone-specific anti-PEG antibodies and methoxy-specific anti-PEG antibodies. Backbone-specific anti-PEG antibodies bind to the backbone of the PEG chain with at least 16 ethylene glycol (EG) units, whereas methoxy-specific anti-PEG antibodies bind to the terminal methoxy group with a few to a few tens of EG units.[13–15] This difference in specificity has been revealed by a variety of methods, such as enzyme-linked immunosorbent assays (ELISAs),[13,16,17] surface plasmon resonance,[18] hemagglutination,[19] acoustic membrane microplate technology,[20] and Western blot analysis.[21] Nevertheless, distinguishing anti-PEG antibodies by specificity is still a difficult task. For instance, in a typical ELISA, a series of PEGs with different chain lengths and terminal groups are attached to proteins or lipids and immobilized onto surfaces of microplates, after which the assay is performed with delicate procedures that include blocking and washing steps for reducing the nonspecific adsorption of proteins (e.g., serum proteins or

enzyme-conjugated secondary antibodies for ELISAs) using appropriate surfactant solutions.[13,16,17] Overall, distinguishing anti-PEG antibodies by specificity in a simple manner remains challenging.

Nanoarchitectonics is an arising concept to construct advanced materials via the fusion of nanotechnology and other research disciplines, including supramolecular chemistry, synthetic chemistry, bio-related technology, and others.[22–25] Herein, we propose the use of nanoarchitectonics-based two-dimensional (2D) cello-oligosaccharide assemblies[26–28] with structural designability and antibiofouling properties as platforms for ELISA. The assemblies have nanoribbon morphologies and are composed of enzymatically synthesized cello-oligosaccharides bearing one-terminal methoxy oligo(ethylene glycol) (OEG) chains with systematically varied numbers of repeating units of 2, 4, 6, and 8; these oligosaccharides were named CEL-EG$_n$ where n corresponds to the number of repeating EG units.[29] The oligosaccharides form monolayer lamellar crystals with an antiparallel molecular arrangement, in which the cello-oligosaccharides adopt the cellulose II allomorph, thereby tethering the OEG ligands to both sides of the nanoribbons in a 2D manner. Because of their 2D shape, the assemblies have a high specific surface area with OEG ligands while remaining sufficiently large for centrifugation, allowing ELISAs to be easily performed by cycles of centrifugation/redispersion of aqueous dispersions of the assemblies. Moreover, these cello-oligosaccharide assemblies have antibiofouling properties against proteins, which minimizes their nonspecific adsorption without the use of a surfactant. By employing this nanoarchitectonics-based oligosaccharide platform that is attractive for use in ELISAs, we successfully distinguished anti-PEG antibodies by specificity for the terminus of PEG in a simple manner (Fig. 1).

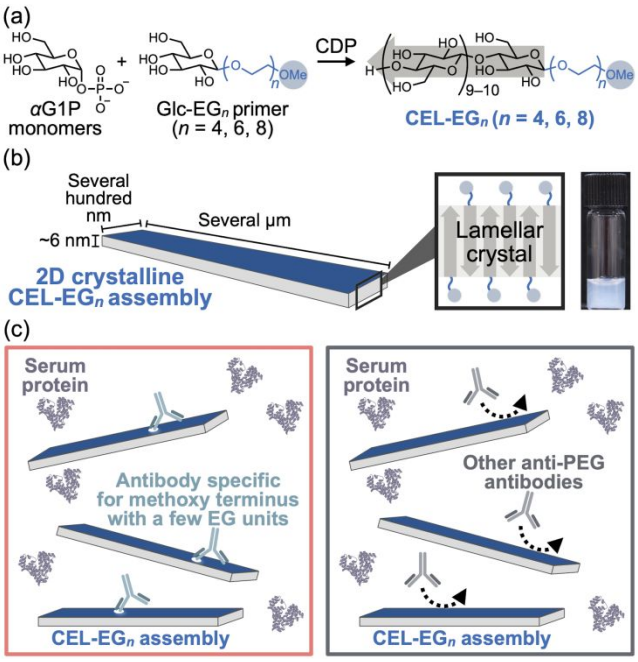

Fig. 1 (a) Synthetic scheme of CEL-EG$_n$ (n = 4, 6, 8) and schematic illustrations for (b) antibiofouling cello-oligosaccharide assemblies tethering one-terminal methoxy OEG ligands and (c) distinguishing anti-PEG antibodies by the assemblies.

2. Materials and methods

2.1 Materials

Bovine serum albumin (BSA, 98%, protease free) was purchased from Wako Pure Chemical Industries. Anti-PEG immunoglobin G (IgG) (clone PEG-B-47, produced in rabbit, monoclonal, ab51257) and horseradish peroxidase (HRP)-conjugated anti-mouse IgG1 (produced in goats, polyclonal, ab97240) were purchased from Abcam. HRP-conjugated anti-mouse IgG (produced in rabbits, polyclonal, A9044), anti-PEG IgG (clone 15-2b, produced in mice, monoclonal, MABS2002-25UG), and anti-PEG IgG (clone 6.3, produced in mice, monoclonal, MABS1966-100UG) were purchased from Sigma–Aldrich Co. HRP-conjugated anti-rabbit IgG (produced in goats, polyclonal, GTX213110-01) was purchased from GeneTex. A rabbit anti-PEG IgG ELISA

kit (PEGG-10) was purchased from Life Diagnostic, Inc. Fetal bovine serum was purchased from BioWest and heated at 56 °C for 30 min to inactivate complement proteins. All other reagents were purchased from Nacalai Tesque. The 96-well plates (clear, flat bottoms) were purchased from Corning. A polypropylene tube (0.2 mL) was purchased from WATSON Bio Lab. Ultrapure water (more than 18.2 MΩ·cm) was obtained from a Milli-Q Advantage A-10 system (Merck Millipore) and used throughout the study.

2.2 Enzyme-catalyzed production of cello-oligosaccharide assemblies

CEL-EG$_n$ (n = 2, 4, 6, and 8) assemblies, a plain cello-oligosaccharide assembly (named CEL-OH), and a cello-oligosaccharide assembly that tethers loop-structured OEG chains with 5 repeating units to the surface (named CEL-EG$_5$-loop assembly) were prepared via cellodextrin phosphorylase (CDP)-catalyzed reverse phosphorolysis reactions and characterized according to our previously reported methods. In brief, for the preparation of the CEL-OH assembly,[30] α-D-glucose 1-phosphate (αG1P) monomers (200 mM), D-glucose primers (50 mM), and CDP (1 U mL^{-1}, derived from *Acetivibrio thermocellus* DSM 1313) were incubated in 500 mM 4-(2-hydroxyethyl)-1-piperazineethanesulfonic acid buffer (pH 7.5) containing 50 μM ethylenediaminetetraacetic acid at 60 °C for 3 d. For purification, the water-insoluble products were washed with ultrapure water through centrifugation (20,400 *g*) and redispersion cycles to remove at least 99.999% of the reaction solution. The obtained products dispersed in ultrapure water were stored at 4 °C before use for matrix-assisted laser desorption ionization time-of-flight (MALDI-TOF) mass spectrometry and atomic force microscopy (AFM). For ^{1}H nuclear magnetic resonance (^{1}H NMR) spectroscopy, the product dispersions were lyophilized. The CEL-EG$_n$[29] and CEL-EG$_5$-loop assemblies[31] were similarly prepared using terminal methoxy OEG chain-bearing

β-D-glucose derivatives (Glc-EG$_n$, 50 mM) and penta(ethylene glycol) with cellobiose units at both ends (Cello-BiP, 25 mM) as primers, respectively. Synthetic schemes of the primers are shown in Scheme S1. The structural properties of cello-oligosaccharide assemblies are summarized in Table 1 and Fig. S1. The average degrees of polymerization (DP) of the cello-oligosaccharide moieties ranged from approximately 9 to 11 (except for CEL-EG$_5$-loop), which were estimated based on the integral ratios of internal (shown as 1' in Fig. S1b) and terminal (shown as 1 in Fig. S1b) anomeric protons in the ^{1}H NMR spectra. The average DPs of cello-oligosaccharide chains in CEL-EG$_5$-loop were estimated to be approximately 6 based on the integral ratios of anomeric protons (shown as 1, 1' in Fig. S1b) and protons from the triazole rings (shown as c in Fig. S1b) in the ^{1}H NMR spectrum. The thicknesses of the assemblies ranged from approximately 5 to 6 nm. The widths of the assemblies were approximately 100 nm to several hundreds of nanometers. The lengths of the assemblies were more than several hundred nanometers and showed large distributions. ^{1}H NMR spectra were recorded at room temperature using an AVANCE III HD spectrometer (500 MHz, Bruker Corporation) for cello-oligosaccharide solutions at concentrations of more than 2% (w/v) in 4% sodium deuteroxide/deuterium oxide. The spectra were calibrated using the water peak (δ = 4.79) as an internal reference. An AXIMA-performance mass spectrometer (Shimadzu Corporation) equipped with a nitrogen laser (λ = 337 nm) and pulsed ion extraction using linear/positive mode was used to acquire the spectra under ambient conditions, followed by calibration with Bradykinin (757.3997 Da), P$_{14}$R (1533.8582 Da), and ACTH (2465.1989 Da). For sample preparation, cello-oligosaccharides were dispersed in acetonitrile/water (1/1, v/v) containing 2,5-dihydroxybenzoic acid (2 mg mL^{-1}) and trifluoroacetic acid (0.01% (v/v)), and the dispersions were deposited onto a sample target plate and dried under ambient conditions. An FT/IR-4100 FTIR spectrometer (Jasco Corporation) was used to measure

attenuated total reflection-Fourier transform infrared (ATR-FTIR) absorption spectra of the lyophilized products at a cumulative number of 100 and a resolution of 2.0 cm^{-1} under ambient conditions. An SPM-9700HT (Shimadzu Corporation) was used to record AFM images in tapping mode under ambient conditions. The samples for the cello-oligosaccharide assemblies were prepared by spin casting the dispersions of the assemblies in water (0.001–0.005% (w/v)) on mica at 600 rpm for 30 min. For the samples of the CEL-EG_4 assemblies after interaction with PEG-B-47, aqueous dispersions of the assembly (0.5% (w/v) in PBS, 10 μL) were mixed with PEG-B-47 solutions (110 ng mL^{-1} in PBS, 100 μL) containing BSA (3.3% (w/v)). After incubation at 25 °C for 1 h, the mixtures were centrifuged (20,400 *g*, 5 min), and 100 μL of the supernatants were removed. Then, 100 μL of ultrapure water was added to redisperse the precipitates, and the dispersions were centrifuged (20,400 *g,* 5 min), and 100 μL of the supernatants were removed. This redispersion and centrifugation cycle was repeated three times to obtain the purified assemblies, which were dispersed in 10 μL of ultrapure water. After adding 490 μL of ultrapure water and mixing by gently pipetting, the dispersions were diluted one hundred-fold. The AFM samples were prepared by spin casting the diluted dispersions on mica at 600 rpm for 30 min.

2.3 Physical adsorption of BSA on the surfaces of the cello-oligosaccharide assemblies in PBS

Aqueous dispersions of the cello-oligosaccharide assemblies in phosphate-buffered saline (PBS, 137 mM NaCl, pH 7.4) were mixed with PBS and BSA solutions in PBS. The final concentrations of cello-oligosaccharide assemblies and BSA were 0.2% (w/v) and 20 μM, respectively. After incubation at 25 °C for 1 h, the mixtures were centrifuged (20,400 *g*, 15 min) to precipitate the assemblies. Ultraviolet–visible (UV–vis) absorption spectra for the supernatants were obtained by using a V-670 spectrometer (JASCO) at room temperature. The BSA concentrations in the

supernatants were estimated based on the absorbance at 280 nm using an appropriate calibration curve. Then, the amounts of protein adsorbed onto the assemblies were estimated by subtracting the amounts in the supernatants from those in the initial solutions. To standardize the amount adsorbed per the unit surface area of the assemblies, the areas for their base planes were estimated from the unit cell area for the cellulose II allomorph (0.65 nm^2 per one cello-oligosaccharide chain) as the apparent total surface area, similar to our previous reports.[32–34] Notably, the surface areas of the edges of the assemblies were ignored because the areas of the base planes appeared to be much greater than those of the edges. The experiments were performed in triplicate.

2.4 ELISAs of anti-PEG antibodies using cello-oligosaccharide assemblies

Aqueous dispersions of cello-oligosaccharide assemblies (0.5% (w/v) in PBS, 10 μL) were mixed with anti-PEG IgG solutions (11 ng mL^{-1} in PBS, 100 μL) containing BSA (3.3% (w/v)) as a blocking reagent in polypropylene tubes. The final concentrations of the assemblies were 0.045% (w/v) unless otherwise stated. After incubation at 25 °C for 1 h, the mixtures were centrifuged (20,400 *g*, 5 min), and 100 μL of the supernatants were removed. Then, 100 μL of PBS was added to redisperse the precipitates, and the dispersions were centrifuged (20,400 *g,* 5 min), and 100 μL of the supernatants were removed. This washing cycle was repeated three times. Aqueous solutions of HRP-conjugated anti-IgG (410 ng mL^{-1} and 440 ng mL^{-1} in PBS for PEG-B-47 and others, respectively, 100 μL) containing BSA (3.3% (w/v)) were added to the resulting mixtures, and the precipitates were dispersed by gentle pipetting. After incubation at 25 °C for 1 h, the mixtures were centrifuged (20,400 *g*, 5 min), and 100 μL of the supernatants were removed. Then, 100 μL of PBS was added to redisperse the precipitates, and the dispersions were centrifuged (20,400 *g,* 5 min), and 100 μL of the supernatants were removed. This washing cycle was repeated three times.

Then, *o*-phenylenediamine solutions (2 mg mL^{-1}) in a McIlvaine buffer solution (pH 4.0) containing hydrogen peroxide (0.11% (w/v)) were added, and the enzymatic reactions were performed at 25 °C for 30 min. After that, 100 μL of sulfuric acid (1.5 M) aqueous solution was added to stop the reactions. Then, 100 μL of each reaction solution was added to a 96-well plate, and the absorbance of each well was measured at 490 nm using a microplate reader (Model 680, Bio-Rad Laboratories, Inc.) at room temperature. For ELISAs of PEG-B-47 at a concentration of 10 ng mL^{-1}, the absorbance values of the reaction solutions diluted twofold were measured. For the other antibodies, the absorbance values of the reaction solutions were measured without dilution. The measured absorbance values were subjected to the subtraction of the absorbance obtained by performing with PBS instead of dispersions of cello-oligosaccharide assemblies. To investigate the dependence of the absorbance value on PEG-B-47 concentration, ELISAs at various final concentrations of PEG-B-47 (1-100 ng mL^{-1}) were similarly performed in which PEG-B-47 was incubated with the CEL-EG_4 assembly and BSA in the absence and presence of 10% fetal bovine serum. The absorbance values of the reaction solutions diluted fivefold were measured and shown without the subtraction. The experiments were performed in triplicate.

2.5 ELISAs of PEG-B-47 using microplates

ELISAs of PEG-B-47 were performed using a commercially available microplate coated with PEGylated BSA, in which the PEG ligand had a molecular weight of 20 kDa and a methoxy terminus, according to the manufacturer's procedure. Aqueous solutions of PEG-B-47 (1–100 ng mL^{-1} in PBS, 100 μL) containing fetal bovine serum (10%) were added into the wells and incubated using a plate shaker (150 rpm, 45 min, 25 °C). After incubation, the solutions were aspirated. The wells were washed with 1× wash solutions (from the kit) five times and struck

sharply onto absorbent paper to remove all residues. HRP-conjugated IgG solutions (from the kit) diluted appropriately were added into the wells and incubated using a plate shaker (150 rpm, 45 min, 25 °C). After incubation, washing processes were similarly performed. The 3,3',5,5'-tetramethylbenzidine solutions (from the kit) were added into the wells to perform the enzymatic reactions with incubation using a plate shaker (150 rpm, 20 min, 25 °C). After the reactions, 100 μL of the stop solutions (from the kit) were added with gentle mixing. The absorbance values of the solutions diluted fivefold were measured within five minutes at 450 nm using a microplate reader at room temperature. The experiments were performed in triplicate.

3. Results and discussion

3.1 Protein adsorption properties of 2D cello-oligosaccharide assemblies

Antibiofouling platforms contribute to the sensitive and selective detection of target bio(macro)molecules under demanding conditions.[35–37] Our previous studies revealed that the CEL-OH assembly showed antibiofouling properties, such as protein nonadsorption.[32–34] In this study, the physical adsorption of BSA, which is the most abundant protein in serum, on the other assemblies was similarly evaluated in PBS. Cello-oligosaccharide assemblies were stably dispersed in PBS at an assembly concentration of 0.5% (w/v) for at least 1 h, which is a sufficient amount of time for evaluating protein adsorption onto the assemblies in the dispersed state (Fig. 2). Fig. S2a shows the UV–vis absorption spectra of BSA solutions before and after incubation with cello-oligosaccharide assemblies at a BSA concentration of 20 μM. The absorption curves hardly changed with all cello-oligosaccharide assemblies used in this study, suggesting that BSA was not adsorbed onto the assemblies. In fact, the amounts adsorbed were estimated to be approximately 0 ng cm^{-2} (the respective estimated amounts adsorbed are shown in Fig. S2b). Thus,

240 OEG-tethering cello-oligosaccharide assemblies were expected to be excellent platforms for the
241 sensitive and selective detection of anti-PEG antibodies.
242

243 **Table 1** Structural properties of the cello-oligosaccharide assemblies used in this study.

Assembly	Average degree of polymerization value of the cello-oligosaccharide moiety[a]	Thickness of the nanoribbons (nm)	Width of the nanoribbons (nm)
CEL-OH	~10	5.8 ± 0.4	Several hundreds
CEL-EG_2	~9	5.4 ± 0.3	Several hundreds
CEL-EG_4	~10	5.9 ± 0.5	Several hundreds
CEL-EG_6	~10	5.9 ± 0.3	100~200
CEL-EG_8	~11	6.3 ± 0.5	~100
CEL-EG_5-loop	~6[b]	5.6 ± 0.2	Several hundreds

244 [a] Estimated from ^{1}H NMR spectra. [b] The value is for one of the two cello-oligosaccharide moieties
245 in a molecular chain.
246

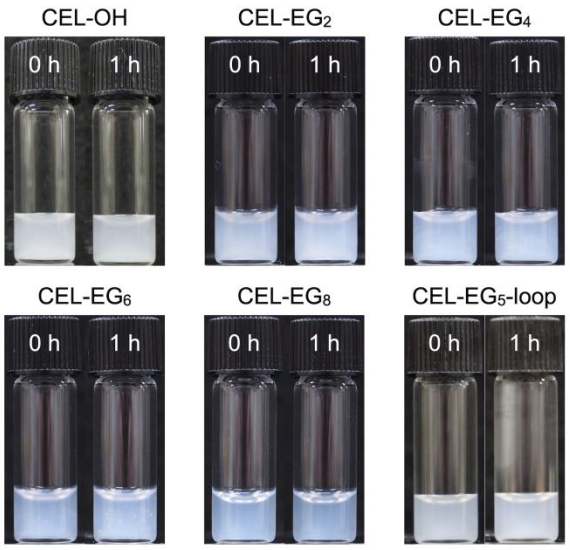

Fig. 2 Photographs of dispersions of cello-oligosaccharide assemblies in PBS at an assembly concentration of 0.5% (w/v) before and after incubation for 1 h.

3.2 Distinguishing anti-PEG antibodies with the cello-oligosaccharide assemblies based on ELISAs

ELISAs of anti-PEG antibodies using microplates require delicate procedures that include blocking and washing steps to decrease the nonspecific adsorption of anti-PEG antibodies, serum proteins, and labeled antibodies (HRP-conjugated secondary antibodies in this assay). On the other hand, in addition to the antibiofouling properties of cello-oligosaccharide assemblies as described in the previous section (Fig. S2), the assemblies were readily precipitated by centrifugation and redispersed in PBS for washing, which suggests the considerable potential of cello-oligosaccharide platforms to perform ELISAs in a simple manner. The present ELISAs were performed in the presence of 3% (w/v) BSA according to a previous study.[38]

One-terminal methoxy PEG is the most frequently used for PEGylation because the chemical reaction conditions are easily controlled.[4] Consequently, anti-PEG antibodies with specificities for not only the backbone PEG chain but also the terminal PEG chain containing a methoxy terminus

(namely, backbone-specific and methoxy-specific anti-PEG antibodies) are known to be induced.[39,40] Properties of anti-PEG antibodies used in this study are shown in Table 2. PEG-B-47 was used as a model target antibody, which requires a terminal methoxy PEG chain with at least three repeating EG units for binding (i.e., methoxy-specific). We applied other anti-PEG antibodies to the assays, 15-2b and 6.3, which require a terminal methoxy PEG chain with at least twelve repeating EG units (i.e., methoxy-specific) and a PEG chain with at least sixteen repeating EG units without terminal groups for binding (i.e., backbone-specific), respectively.

Fig. 3 shows the absorbance values at 490 nm for the products derived from HRP conjugated to the secondary antibodies at an anti-PEG antibody concentration of 10 ng mL^{-1} using cello-oligosaccharide assemblies. The absorbance values correspond to the levels of anti-PEG antibodies detected. In the case of the CEL-OH and CEL-EG_2 assemblies, the absorbance values were very low regardless of the antibody clone, indicating that the cello-oligosaccharide assemblies hardly adsorbed or detected the anti-PEG antibodies applied in the ELISAs (Fig. 3a–b). In the case of the CEL-EG_n assemblies (n = 4, 6, and 8), absorbance values were clearly observed for PEG-B-47, indicating the successful detection of PEG-B-47 (Fig. 3c–e). Considering the specificity of PEG-B-47 for the terminal methoxy PEG chain with at least three repeating EG units, it was plausible that the absorbance values drastically changed from the CEL-EG_2 to CEL-EG_4 assemblies. HRP-conjugated secondary antibodies were hardly adsorbed onto the cello-oligosaccharide assemblies used in this study (Fig. S3), supporting the conclusion that the assemblies detected PEG-B-47 with high reliability based on ELISA. Moreover, the absorbance values were very low for 15-2b and 6.3, indicating that the CEL-EG_n assemblies (n = 4, 6, and 8) hardly detected the anti-PEG antibodies (Fig. 3c–e), possibly due to the requirements of more repeating EG units for the binding of 15-2b and 6.3. When the CEL-EG_5-loop assembly, in which the OEG ligands do not have a

methoxy terminus, was used, anti-PEG antibodies were not detected (Fig. 3f). These results demonstrate that ELISAs using terminal methoxy OEG-tethering cello-oligosaccharide assemblies allow for simply distinguishing anti-PEG antibodies by specifically identifying the PEG terminus.

For PEG-B-47, the absorbance values for CEL-EG$_n$ assemblies (n = 4, 6, and 8) gradually decreased with increasing number of EG units, suggesting that the binding of the anti-PEG antibodies to the OEG ligands on the assemblies was suppressed with increasing OEG chain length. This decrease was possibly derived from the steric hindrance and conformational restriction of the surface OEG ligands. Considering that the assemblies are monolayer lamellar crystals with the cellulose II allomorph, the area occupied by an OEG ligand on the assemblies can be estimated to be 0.65 nm^2 (Fig. S4).[41] On the other hand, the Flory radii for the EG$_4$, EG$_6$, and EG$_8$ chains were estimated to be 0.76 nm, 0.97 nm, and 1.2 nm, respectively.[42] These estimations suggest that the OEG ligands interfere with each other to restrict their conformational freedoms as the number of EG units increases. In other words, the steric hindrance of adjacent OEG ligands and the possible conformational changes likely interfere with the binding of the anti-PEG antibodies to the longer OEG ligand. It was therefore determined that the OEG ligand length on the surfaces of the cello-oligosaccharide assemblies was an important factor for the effective detection of anti-PEG antibodies.

Table 2 Properties of the anti-PEG antibodies used in this study.

Antibody name	Preferred PEG structure for antibody binding	Preferred number of repeating EG units for antibody binding
PEG-B-47[43]	Terminus PEG chain containing a methoxy terminus	≥3
15-2b[13]	Terminus PEG chain containing a methoxy terminus	≥12
6.3[13]	Backbone PEG chain	≥16

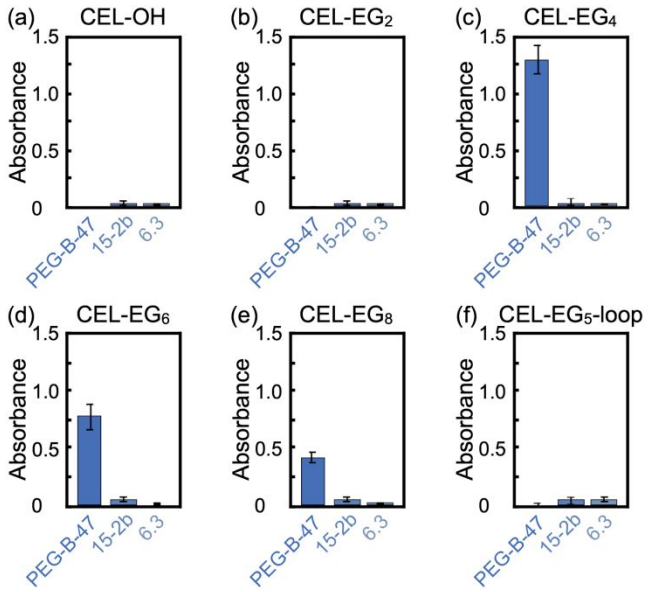

Fig. 3 ELISAs of anti-PEG antibodies using (a) CEL-OH, (b) CEL-EG_2, (c) CEL-EG_4, (d) CEL-EG_6, (e) CEL-EG_8, and (f) CEL-EG_5-loop at an anti-PEG antibody concentration of 10 ng mL^{-1} and an assembly concentration of 0.045% (w/v).

The concentration of PEG-B-47 used for ELISAs with the CEL-EG_4 assemblies in PBS varied over the range of 0–100 ng mL^{-1} (Fig. 4). The absorbance values increased with increasing antibody concentration in the range of 0–50 ng mL^{-1}, almost reaching a plateau above 50 ng mL^{-1}, resulting in a saturation profile (Fig. 4a). This observation possibly suggests that the anti-PEG

316 antibodies bind to the EG_4 ligand on the assembly surface in a monolayer. In fact, the atomic force
317 microscopy observations revealed nanometer-sized granules that could possibly be assigned to
318 PEG-B-47 on the assembly surface (Fig. S5). The absorbance value with 100 ng mL^{-1} PEG-B-47
319 slightly decreased compared with that at 50 ng mL^{-1}. This might be attributed to a decrease in the
320 effective surface area of the assembly based on partial aggregation of the assembly with anti-PEG
321 antibodies (namely, crosslinking of the assemblies with anti-PEG antibodies).[44]
322 Assuming that the dependence of the absorbance value on the PEG-B-47 concentration was
323 an adsorption isotherm, the profile in the range of 0–50 ng mL^{-1} was fitted to the Langmuir
324 adsorption model with a coefficient of determination (R^2) value of 1.00 (Fig. S6). The apparent
325 dissociation constant (K_d) was estimated from the fitting to be 0.325 nM (this constant is discussed
326 below). In the range of 0–10 ng mL^{-1}, the plots were fitted to a linear equation with an R^2 value of
327 0.997 (Fig. 4b), suggesting that the present ELISAs can be used for quantitative anti-PEG antibody
328 detection in the concentration range. Using the slope of the linear plot and the standard deviation
329 (σ) of the absorbance value at an antibody concentration of 0 ng mL^{-1}, the limit of detection (LOD)
330 value (= 3σ/slope)[45] was estimated to be 0.065 ng mL^{-1}. Taken together, these results suggested
331 that these cello-oligosaccharide platforms have great potential to efficiently distinguish anti-PEG
332 antibodies and sensitively detect a specific anti-PEG antibody based on a simple ELISA method.
333

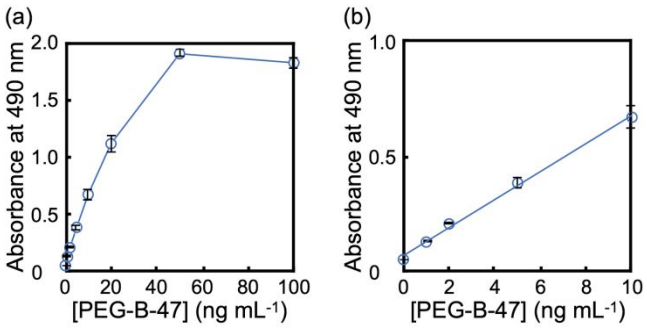

Fig. 4 (a) ELISAs of PEG-B-47 using 0.045% (w/v) CEL-EG_4 assembly at different PEG-B-47 concentrations. (b) Linear fitting in the concentration range of 0–10 ng mL^{-1}.

3.3 ELISAs of anti-PEG antibodies in the presence of serum

An essential question when analyzing the characteristics of anti-PEG antibodies is whether our assays can quantify antibodies in serum samples for future practical applications. To evaluate the practicability of the present ELISAs using antibiofouling cello-oligosaccharide platforms, the concentration of PEG-B-47 in the ELISAs using the CEL-EG_4 assemblies was changed in the range of 0–100 ng mL^{-1} in the presence of 10% fetal bovine serum as a model serum (Fig. 5). The absorbance values increased with increasing anti-PEG antibody concentration in the range of 0–50 ng mL^{-1} and then almost reached saturation above 50 ng mL^{-1} (Fig. 5a), suggesting monolayer adsorption of the anti-PEG antibodies on the assembly surface even in the presence of serum. Monolayer adsorption was supported by the fact that the profile in the range of 0–50 ng mL^{-1} fit to the Langmuir adsorption model with an R^2 value of 0.998 (Fig. S7). The apparent K_d was estimated from the fitting to be 0.219 nM, which was almost the same as that in the absence of serum. Moreover, the plot was fitted to a linear equation with an R^2 value of 0.995 in the anti-PEG antibody concentration range of 0–10 ng mL^{-1} (Fig. 5b). The LOD was estimated to be 0.10 ng mL^{-1}, which is comparable to that in the absence of serum (0.065 ng mL^{-1}). Therefore, serum components such as proteins hardly affect the binding of anti-PEG antibodies to OEG ligands on

354 cello-oligosaccharide assemblies. Notably, the detectable and quantifiable range of anti-PEG
355 antibody concentrations was estimated to be 0.10–10 ng mL^{-1}, which covered the range of the
356 concentrations required for clinical analysis of the effects of anti-PEG antibodies on the
357 pharmacokinetics and/or safety of PEGylated therapeutics.[6] It appears that the antibiofouling
358 properties of these cello-oligosaccharide platforms allow for the quantitative detection of specific
359 anti-PEG antibodies even in the presence of serum.
360

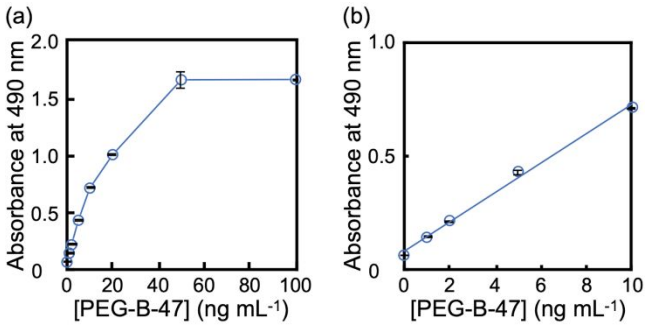

361

362 **Fig. 5** (a) ELISAs of PEG-B-47 using 0.045% (w/v) CEL-EG_4 assembly at different PEG-B-47
363 concentrations in the presence of 10% fetal bovine serum. (b) Linear fitting in the concentration
364 range of 0–10 ng mL^{-1}.
365

366 The LOD of PEG-B-47 by the cello-oligosaccharide platforms was almost the same as that
367 (0.050 ng mL^{-1}) for conventional ELISAs using commercially available microplates covered with
368 PEGylated BSA, of which PEG had a molecular weight of 20 kDa and a methoxy terminus (Fig.
369 S8). Nevertheless, the present ELISAs using the antibiofouling cello-oligosaccharide platforms
370 required simple procedures, including centrifugation/redispersion cycles, without the need for
371 delicate techniques. Overall, it is suggested that the simple ELISAs using nanoarchitectonics-based
372 antibiofouling cello-oligosaccharide platforms presented here have great potential for practical
373 applications.

4. Conclusions

In conclusion, distinguishing anti-PEG antibodies in a simple manner was demonstrated by using antibiofouling 2D cello-oligosaccharide assemblies tethering one-terminal methoxy OEG ligands. The assemblies were well dispersed in PBS, and the nonspecific adsorption of proteins on the assemblies was very low level, making our assays not only reliable but also simple. The anti-PEG antibodies were successfully distinguished based on our ELISAs using specific OEG ligand-tethering crystalline assemblies. Notably, the quantitative detection of a particular methoxy-specific anti-PEG antibody was successfully performed even under practical conditions with serum, which hardly interfere with quantification. Considering that the ELISAs presented here can be simply performed by centrifugation/redispersion cycles without the need for delicate techniques and that mammalian body fluids do not normally contain enzymes that degrade cello-oligosaccharides (e.g., cellulases), the present study opens a new avenue for the analysis of the binding characteristics of anti-PEG antibodies in biological samples. Specifically, immunogenicity of PEGylated therapeutics under use and development can be investigated reliably and simply by using cello-oligosaccharide assemblies, which potentially contribute to designing the improved therapeutics with excellent therapeutic efficacy and clinical safety.

Declaration of competing interests

The authors declare no competing financial interests.

Data availability

Data will be made available on request.

Acknowledgments

The authors are grateful for the financial support to T. Serizawa from Grants-in-Aid for Scientific Research from the Japan Society for the Promotion of Science (JP18H02029 and JP21H01996) and Grants-in-Aid for Scientific Research on Innovative Areas (Aquatic Functional Materials) from the Ministry of Education, Culture, Sports, Science and Technology, Japan (JP20H05208, JP19H05714, and JP22H04528). The authors wish to thank Mr. M. Nishiura, Ms. R. Murase, and Ms. N. Hayakawa (DKS Co. Ltd.) for cooperative research and fruitful discussions. K. Sugiura acknowledges financial support from the JST SPRING, grant number JPMJSP2106.

References

1. R. Duncun, *Nat. Rev. Drug Discov.*, 2003, **2**, 347–360.
2. I. Ekladious, Y. L. Colson and M. W. Grinstaff, *Nat. Rev. Drug Discov.*, 2019, **18**, 273–294.
3. P. Haag and F. Kratz, *Angew. Chem. Int. Ed.*, 2006, **45**, 1198–1215.
4. G. T. Kozma, T. Shimizu, T. Ishida and J. Szebeni, *Adv. Drug Deliv. Rev.*, 2020, **154-155**, 163–175.
5. B.-M. Chen , T.-L. Cheng and S. R. Roffler, *ACS Nano*, 2021, **15** , 14022–14048.
6. Q. Yang, T. M. Jacobs, J. D. McCallen, D. T. Moore, J. T. Huckaby, J. N. Edelstein and S. K. Lai, *Anal. Chem.*, 2016, **88**, 11804–11812.
7. J.-L. Fang, F. A. Beland, Y. Tang and S. R. Roffler, *Toxical*. *Rep*., 2021, **8**, 148–154.
8. K. Shiraishi, M. Hamano, H. Ma, K. Kawano, Y. Maitani, T. Aoshi, K. J. Ishii and M. Yokoyama, *J. Control. Release*, 2013, **165**, 183–190.
9. K. Shiraishi and M. Yokoyama, *Sci. Technol. Adv. Mater.*, 2019, **20**, 324–336.

10. W.-A. Chen, D.-Y. Chang, B.-M. Chen, Y.-C. Lin, Y. Barenholz and S. R. Roffler, *ACS Nano*, 2023, **17**, 5757–5772.
11. M. D. McSweeney, M. Mohan, S. P. Commins and S. K. Lai, *Front. Allergy*, 2021, **2**.
12. J. D. Vrieze, *Science*, 2021, **371**, 10–11.
13. W.-W. Lin, Y.-C. Hsieh, Y.-A. Cheng, K.-H. Chuang, C.-C. Huang, C.-H. Chuang, I.-J. Chen, K.-W. Cheng, Y.-C. Lu, T.-C. Cheng, Y.-T. Wang, S. R. Roffler and T.-L. Cheng, *Anal. Chem.*, 2016, **88**, 12371–12379.
14. J. T. Huckaby, T. M. Jacobs, Z. Li, R. J. Perna, A. Wang, N. I. Nicely and S. K. Lai, *Commun. Chem.*, 2020, **3**, 124.
15. M.-T. T. Nguyen, Y.-C. Shin, M.-H. Lin, S. R. Roffler, C.-Y. Hsiao, T.-L. Cheng, W.-W. Lin, E.-C. Lin, Y.-J. Jong, C.-Y. Chang and Y.-C. Su, *Commun. Chem.*, 2022, **5**, 88.
16. K.-H. Chuang, C.-H. Kao, S. R. Roffler, S.-J. Lu, T.-C. Cheng, Y.-M. Wang, C.-H. Chuang, Y.-C. Hsieh, Y.-T. Wang, J.-Y. Wang, K.-Y. Weng and T.-L. Cheng, *Macromolecules*, 2014, **47**, 6880–6888.
17. G. T. Kozma , T. Meszaros , I. Vashegyi , T. Fulop , E. Orfi , L. Dezsi , L. Rosivall , Y. Bavli , R. Urbanics , T. E. Mollnes , Y. Barenholz and J. Szebeni, *ACS Nano*, 2019, **13** , 9315–9324.
18. P. Zhang, F. Sun, H.-C. Hung, P. Jain, K. J. Leger and S. Jiang, *Anal. Chem.*, 2017, **89**, 8217–8222.
19. R. P. Garay, R. EI-Gewely, J. K. Armstring, G. Garratty and P. Richette, *Expert Opin. Drug Deliv.*, 2012, **9**, 1319–1323.
20. H. Dong, J. R. Mora, C. Brockus, S. D. Chilewski, R. Dodge, C. Merrifield, W. M. Dickerson and B. DeSilva, *AAPS J.*, 2015, **17**, 1511–1516.

21. K. Sroda, J. Rydlewski, M. Langner, A. Kozubek, M. Crzybek and A. F. Sikorski, *Cell. Mol. Biol. Lett.*, 2005, **10**, 37–47.
22. V. Karthick, L. Kumar Shrestha, V. G. Kumar, P. Pranjali, D. Kumar, A. Pal and K. Ariga, *Nanoscale*, 2022, **14** , 10630–10647.
23. K. Ariga, *Mater. Chem. Front.*, 2017, **1**, 208–211.
24. K. Ariga, *Nanoscale Horiz.*, 2021, **6**, 364–378
25. M. B. Avinash and T. Govindaraju, *Nanoscale*, 2014, **6**, 13348–13369.
26. Y. Hata and T. Serizawa, *J. Mater. Chem. B*, 2021, **9**, 3944–3966.
27. Y. Hata and T. Serizawa, *Bull. Chem. Soc. Jpn.*, 2021, **94**, 2279–2289.
28. K. Sugiura, M. Saito, T. Sawada, H. Tanaka and T. Serizawa, *ACS Sustainable Chem. Eng.*, 2022, **10**, 13484–13494.
29. T. Nohara, T. Sawada, H. Tanaka and T. Serizawa, *Langmuir*, 2016, **32**, 12520–12526.
30. T. Serizawa, M. Kato, H. Okura, T. Sawada and M. Wada, *Polym. J.*, 2016, **48**, 539–544.
31. K. Sugiura, T. Sawada, H. Tanaka and T. Serizawa, *Polym. J.*, 2021, **53**, 1133–1143.
32. T. Serizawa, T. Maeda and T. Sawada, *ACS. Macro. Lett.*, 2020, **9**, 301–305.
33. T. Serizawa, S. Yamaguchi, M. Amitani, S. Ishii, H. Tsuyuki, Y. Tanaka, T. Sawada, I. Kawamura, G. Watanabe and M. Tanaka, *Colloids Surf. B*, 2022, **220**, 112898.
34. T. Nohara, T. Sawada, H. Tanaka and T. Serizawa, *J. Biomater. Sci. Polym. Ed.*, 2017, **28**, 925–938.
35. C. Jiang, G. Wang, R. Gein, N. Liu, X. Luo and J. J. Davis, *Chem. Rev.*, 2020, **120**, 3852–3889.
36. S. Zhu, D. Wang, M. Li, C. Zhou, D. Yu and Y. Lin, *J. Mater. Chem. B*, 2022, **10**, 2113–2125.
37. O. Wang, T. Shi, M. Wan, J. Wei, F. Wang and C. Mao, *J. Mater. Chem.*, *B* 2021, **9**, 283–

294.

38. M. Hanamura, T. Sawada and T. Serizawa, *ACS Sustainable Chem. Eng.*, 2021, **9**, 5684–5692.
39. Y. Hashimoto, T. Shimizu, Y. Mima, A. S. A. Lila, T. Ishida and H. Kiwada, *Toxicol. Appl. Pharmacol.*, 2014, **277**, 30–38.
40. Y.-C. Su, B.-M. Chen, K.-H. Chuang, T.-L. Cheng and S. R. Roffler, *Bioconjugate Chem.*, 2010, **21**, 1264–1270.
41. M. Hiraishi, K. Igarashi, S. Kimura, M. Wada, M. Kitaoka and M. Samejima, *Carbohydr. Res.*, 2009, **344**, 2468–2473.
42. H. Lee, A. H. de Vries, S.-J. Marrink and R. W. Pastor, *J. Phys. Chem. B*, 2009, **113**, 13186–13194.
43. M. G. Saifer, L. D. Williams, M. A. Sobczyk, S. J. Michaels and M. R. Sherman, *Mol. Immunol.*, 2014, **57**, 236–246.
44. T. Miyata, N. Asami and T. Uragami, *Nature*, 1999, **399**, 766–769.
45. J. Uhrovčík, *Talanta*, 2014, **119**, 178–180.